Bull. Mater. Sci., Vol. 40, No. 2, April 2017, pp. 253–262. © Indian Academy of Sciences.
DOI 10.1007/s12034-017-1373-5

Electrical and optical properties of ZnO–WO_3 nanocomposite and its application as a solid-state humidity sensor

VANDNA SHAKYA*, N K PANDEY, SUNEET KUMAR MISRA and AKASH ROY
Sensors and Materials Research Laboratory, Department of Physics, University of Lucknow, Lucknow 226007, India

MS received 19 May 2015; accepted 2 September 2016

Abstract. **This study reports the humidity sensing characteristics of ZnO–WO_3 nanocomposite. Pellet samples of 0–5 weight% ZnO in WO_3 were sintered from 300 to 600°C. When exposed to humidity, the resistance of the sensing samples was found to decrease with increase in relative humidity (RH). Five percent ZnO-doped WO_3 showed maximum sensitivity of 20.95 MΩ/%RH in 15–95% RH range. Sensor parameters like reproducibility, aging, hysteresis, response and recovery times were also studied. Sensing mechanism is discussed in terms of sintering temperature, composition and crystallite size of the sensing element. It was observed that sensing mechanism is strongly based on annealing temperature and percentage of doping. The sensing samples have also been investigated by X-ray diffraction, scanning electron microscope (SEM) and Raman spectroscopy. The crystalline size of the sample was identified by powder X-Ray Diffraction data. The SEM analysis was used to study the surface morphology. The structure, phase and the degree of crystallinity of the materials were examined by Raman spectroscopy.**

Keywords. **Sensor; humidity; adsorption; hysteresis; porous.**

1. Introduction

Humidity monitoring and controlling devices have significant importance in industrial, environmental, agricultural and medical fields. Resistive humidity sensors are the devices that transduce humidity change to resistance change. Three groups of materials have been used and reported for resistive humidity measurements: ceramics, polymers and electrolytes. Ceramics such as WO_3, ZnO, SnO_2, Al_2O_3, TiO_2, etc. are most investigated sensing materials for relative humidity (RH) sensors. Nowadays, varieties of humidity sensor that are available or under review process for development in various research institutions are RH-type sensors. We can categorize these type of sensors into three classes, including ceramic type (semiconductor), organic polymer-based sensors and organic/inorganic hybrid sensors (polymer/ceramic). Humidity sensors that are currently manufactured by using nanowires, nanofibres, nanorods and p–n heterojunctions are subclasses of the ceramic (inorganic) type.

The intrinsic characteristics of ceramic material namely, reproducibility of the electrical properties, mechanical strength, chemical and physical stability have been a centre of attraction nowadays. These type of materials possess a unique structure consisting of grains, grain boundary surfaces and pores, which make them suitable for adsorption of water molecules because of the high surface exposure [1]. Generally, metal oxides can be classified into two types, non-transition and transition; the binary transition-metal oxides (e.g., TiO_2, V_2O_5, WO_3) with d^0 configuration and post-transition oxides (e.g., ZnO, SnO_2) with d^{10} configuration. Transition-metal oxides behave differently because the energy difference between a cation d^n configuration and either a d^{n+1} or d^{n-1} configurations is often rather small [2]. Due to small energy differences the transition metal oxides are utilized for sensing applications, because they can form various oxidation states on the surface of metallic oxides.

Tungsten oxides (WO_3) are a strong candidate used for sensing purpose, with high sensitivity and also long-term stability [3]. Consequently, this system has been examined in substantial detail using several categories of material like bulk ceramic [4], thin film [5–8] and thick film [9]. Tungsten trioxide (WO_3) has been investigated intensively because of its intriguing structures, physical and chemical properties [10–13], and potential applications [14–18]. One of the elementary defects in tungsten oxide structure, as in most metal oxide, is the lattice oxygen vacancy, where an oxygen atom is lacking from the normal lattice site. The octahedral variation in corners sharing to edge sharing lattice with the formation of crystallographic shear planes built up of edges and plane sharing structures, which corresponds to particle replacement of W^{6+} to W^{5+} and W^{4+} ions. This leads to the formation of non-stoichiometric tungsten oxides WO_{3-x} and strongly influences its electronic properties [19]. ZnO is an attractive semiconductor oxide for sensing purpose having a wide bandgap and is known for its *n*-type conduction due to the presence of oxygen vacancies [20,21]. It is observed that the sensitivity of pure sensing material increases after doping of ZnO because the amount of highest carrier concentration of holes and electrons attained to about 10^{19} and 10^{20} cm^{-3}, respectively, were reported [22].

*Author for correspondence (vandna647@rediffmail.com)

Dewyani Patil *et al* [23] synthesized poly(2, 5-dimethoxyaniline)/WO_3 (PDMA/WO_3) composites by mechanical mixing method and investigated the humidity sensing properties. The composite with 30 weight% of WO_3 changes linearly over the humidity range 23–84% and RH shows maximum percentage response factor (∼651 at 87% RH), quick response (humidification, 27 s and desiccation, 136 s), narrow hysteresis (∼5%) and an excellent repeatability of the response [23]. Yadav *et al* [24] reported the synthesis and characterization of ZnO–TiO_2 nanocomposite and its application as humidity sensor. ZnO was prepared by conventional precipitation method using sodium hydroxide. The ZnO–TiO_2 nanocomposite exhibits its highest average sensitivity of 18 MΩ/%RH over the entire range of %RH, i.e., from 10 to 95% RH at room temperature (19°C). The average size of nanoparticles is found to be a minimum in the range 50–200 nm at 19°C temperature.

Sundaram and Nagaraja [25] report that lead (II) tungstate and zinc (II) tungstate were prepared by a solution route method and sintered at 973 K in the form of cylindrical discs. The composites were subjected to d.c. resistance measurements as a function of RH in the range 5–98% RH, achieved by different water vapour buffers thermostated at room temperature. The composites have the highest humidity sensitivity factor of 17615 ± 3000 and 2666 ±550, respectively. The response and recovery time for these humidity sensing composites were good. Noubeil Guermat *et al* [26] report the study of humidity-sensitive and electrical properties of plasma polymerization of hexamethyldisiloxane (pp-HMDSO) thin film-based sensors. The humidity sensitive film was deposited by glow discharge at low frequency power (19 kHz) in a capacitive-coupled parallel plate plasma reactor. The deposited film sensor exhibited a small hysteresis (2% RH) and fast response (8 and 34 s for adsorption and desorption between 35 and 95% RH, respectively). Md Sin *et al* [27] have reported about the electrical characteristics of aluminium (Al)-doped zinc oxide (ZnO) thin film for high sensitivity humidity sensors. Parameter 0.6 at% aluminium-doped ZnO showed high sensitivity of 2.32 MΩ/%RH and suitable for humidity sensor. Photoluminescence showed emissions band with two peaks centred at about 380 (ultraviolet (UV)) and 600 nm (green) at room temperature (table 1).

Table 1. Variations in average sensitivity with different sensing materials.

Materials	Average sensitivity (MΩ/%RH)	Hysteresis	Reference
ZnO–Nb_2O	19	5%	[28]
ZnO–TiO_2	9.08	1.90%	[29]
WO_3–SnO_2 HNS	16.2	—	[30]
ZnO	11.13	Small	[31]
Ag-doped WO_3	2.14	1.00%	[32]
Cu_2O-doped ZnO	4.78	3.78%	[33]

The above developments inspired us to prepare suitable material for the humidity sensing applications with improved sensitivity. In our earlier study, we have reported the morphological and RH sensing studies of pure WO_3 and WO_3–ZnO (samples WZ-10, WZ-25 and WZ-50) nanocomposite prepared by solid-state reaction route sintered in air at temperature 300–500°C [34]. The present paper reports the electrical and optical properties of ZnO–WO_3 (samples ZW-1, ZW-2, ZW-3, ZW-4 and WZ-5) nanocomposite and its application as a solid-state humidity sensor sintered in air at temperature 300–600°C. The aim of this study is to examine the variation induced on the sensing element by ZnO doping. The nature of the changes analysed is two-fold. On the one hand, morphological and crystalline variations are studied and, on the other hand, variations in response to humidity are investigated. Scanning electron microscopy (SEM), X-ray diffraction (XRD) and Raman spectra have been used to study the morphological variation, to investigate the changes in the crystalline structure and to examine the structure, phase and components of materials, respectively. The sensitivity in present case is higher for ZW-5 (20.95 MΩ/%RH) than the sensing element WZ-50 (1.20 MΩ/%RH) in earlier case. The present study also indicates that there is an improvement in the sensor performance in terms of repeatability and hysteresis. A positive humidity sensing phenomenon was observed between pure WO_3 and ZnO-doped WO_3, which might explain the doping and temperature dependency of the sensing material that was not found in the earlier case.

2. Sample preparation and experimental process

The nanocomposite sample of ZnO–WO_3 was prepared through solid-state reaction route. The starting materials taken were WO_3 (Loba Chemie, 99.99% pure) and 1 weight% (sample ZW-1), 2 weight% (sample ZW-2), 3 weight% (sample ZW-3), 4 weight% (sample ZW-4) and 5 weight% (sample ZW-5) of ZnO powder (Loba Chemie, 99.9%) added in WO_3. Polyvinyl alcohol (10% weight) is added as binder to increase the strength of the sample. Mixed powder was ground to uniformity for 3 h. Then the resultant powder was pressed into pellet shape by uniaxially applying pressure of 267 MPa in a hydraulic press machine (M.B. Instruments, Delhi, India) at room temperature. The prepared pellet samples were in disc shape, having a diameter of 15 mm and 2.3 mm in thickness. Pressed powder pellets were sintered in air at 300–600°C for 3 h in an electric muffle furnace (Ambassador, India) and cooled to room temperature. After sintering, each sensing sample was placed in the same humidity chamber and its sensing outputs were obtained under different humidity levels. Figure 1 shows the schematic diagram of humidity sensing apparatus. Saturated salt solution of potassium sulphate was used as a humidifier and potassium hydroxide as de-humidifier. Inside the humidity chamber, a thermometer (±1°C) and standard hygrometer (±1% RH, digital) were placed for the purpose of

calibration. Electrical characteristic of the sensors was measured by a multifunctional digital multimeter (±0.001 MΩ, VC-9808) at variant humidity environments. The electrical resistance of the sensing elements in the form of pellets have been measured normal to the cylindrical surfaces of the pellets at different RH levels by two-probe method. The electrical contacts were made on the surface of pellets by means of two thin copper sheets. Given high resistivity of materials under consideration, potential inaccuracy due to contact resistance was assumed negligible. The surface contact area of all sensing elements with electrodes was 113.11 mm^2 and the cylindrical surface area that was exposed to the humidity in the chamber was also 113.11 mm^2. These values were kept constant for all the sensing elements. Experimental samples were electrically connected to a power supply and resistance metre in series. After studying humidity sensing properties, sensing elements were kept in laboratory environment and their humidity sensing characteristics were regularly monitored. To see the effect of aging, sensing properties of these elements were examined again in the humidity chamber after 8 months. Stability of sensing elements was checked by keeping the sensing element at fixed values of %RH in the chamber and the values of resistance were recorded as function of time. Samples of pure WO_3 (0% ZnO-doped WO_3), 1% ZnO-doped WO_3, 2% ZnO-doped WO_3, 3% ZnO-doped WO_3, 4% ZnO-doped WO_3 and 5% ZnO-doped WO_3 have been labelled ZW-0, ZW-1, ZW-2, ZW-3, ZW-4 and ZW-5, respectively.

3. Principle of operation

In ceramic sensors, resistance of sensor decreases with increase in RH due to physisorption and capillary condensation of water molecules on the surface of the material (figure 2). Water molecules act as electron donating gas and their chemisorption increases or decreases electronic conductivity depending on whether the material is n- or p-type semiconductor. When moisture comes in contact with ZnO–WO_3 nanocomposite, water molecules irreversibly chemisorb on oxide surface [35–37]. The chemisorbed layer can be thermally removed by increasing the surrounding

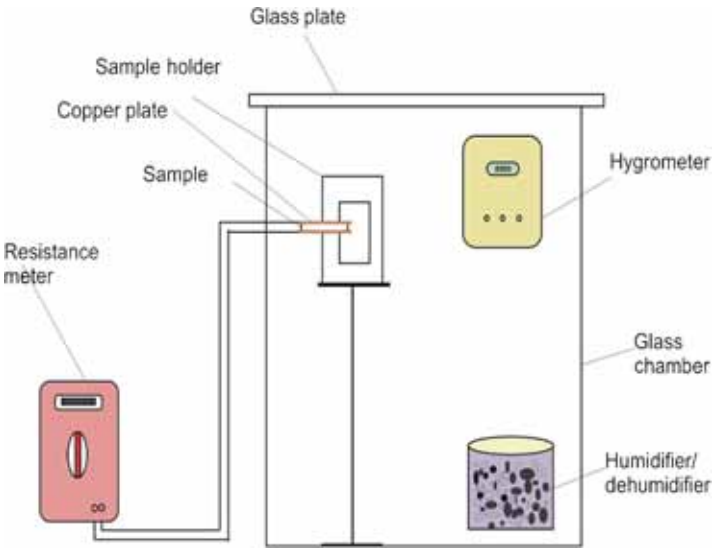

Figure 1. Schematic diagram of humidity sensing apparatus.

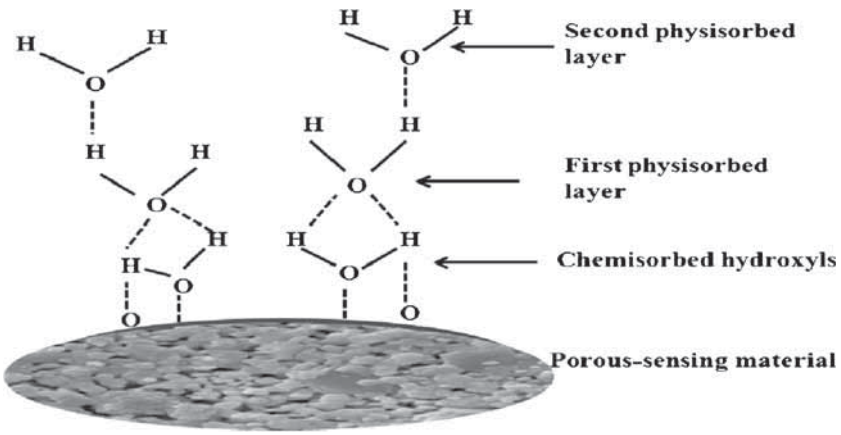

Figure 2. Sensing mechanism of solid-state humidity sensor.

temperature. For transition-metal ion M^+ the irreversible reaction for the first layer may be written as

$$M^+ + H_2O \rightarrow M\text{–}OH + H^+ \quad (1)$$

Subsequent water layers are physically adsorbed on the first chemisorbed layer. The physisorbed water layer is bound by weak hydrogen bonding on the chemisorbed layer and may be removed by decreasing humidity. The chemisorbed water molecule attracts and breaks oxygen to hydrogen bonds of physisorbed water molecules by following mechanism proposed by Friot *et al* [38] and Anderson and Parks [39]:

$$2H_2O \leftrightarrow H_3O^+ + OH^- \quad (2)$$

This physisorbed layer contributes mostly to humidity sensitive conduction of metal oxide ceramics leading to the conduction of electrons at the pure WO_3 or ZnO–WO_3 nanocomposite surface that causes decrease in resistance with increase in RH.

4. Results and discussion

4.1 *Humidification graphs*

Figure 3 shows the humidification graphs for the sensing samples ZW-0, ZW-1, ZW-2, ZW-3, ZW-4 and ZW-5 for the sintering temperature 600°C in terms of resistance *vs.* RH at room temperature repeated over many cycles. Figure 3 shows large decrease in the value of the resistance against initial values of RH from 15 to 40% RH, while in 40–95% RH range the decrease in resistance is slow. The maximum sensitivity of 20.95 MΩ/%RH has been found for the sensing element ZW-5 as compared to the sensitivity of the sensing elements ZW-0, ZW-1, ZW-2, ZW-3 and ZW-4. As observed from figure 3, the value of sensitivity increases with increase in the percentage of ZnO in WO_3.

Higher porosity increases surface-to-volume ratio of the materials and enhances diffusion rate of water into or out-off the porous structure; thus, at high humidity (>40% RH) the proton hopping and the ionic conduction increase surface conductivity while at low humidity (<40% RH) there is no effective protonic conduction [40]. Overall, the resistance of the ceramic decreases with an increase in humidity [41]. The decrement in resistance or increase of conductance also occurs due to the variation of grain boundary barrier height inside the ceramics. In this case the adsorption of water molecules interpenetrated at WO_3 surface can decrease the height of potential barriers at the surface of WO_3 grains and at the surface of necks between WO_3 grains. Therefore the size of the depletion regions in the vicinity of the necks in the direction of electric field is lowered and conductance of ceramics is increased. Penetrated water molecules can promote the decrease in the barrier heights of grain boundary potential barriers exponentially; therefore slight decrease in grain boundary barriers height on RH can cause strong decrease in resistance (or increase of conductance). This is schematically shown in figure 4. In this case the conductance can change with the value of RH exponentially [42].

Sensitivity of humidity sensor is defined as the change in resistance (ΔR) of sensing element per unit change in RH (ΔRH%). For calculation of sensitivity, humidity from 15 to 95% RH was divided in equal intervals of 5% RH each. The difference in the value of the resistance for each of this interval was calculated and then divided by 5. An average was taken for all these calculated values. Formula for calculation

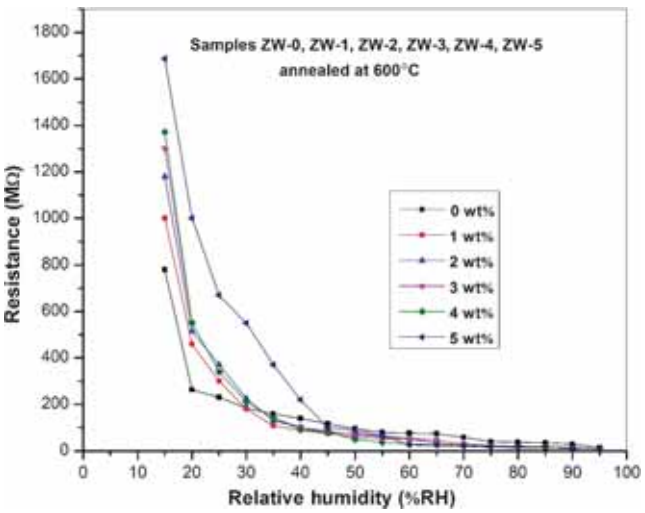

Figure 3. Humidification graph for samples ZW-0, ZW-1, ZW-2, ZW-3, ZW-4 and ZW-5 for sintering temperature 600°C.

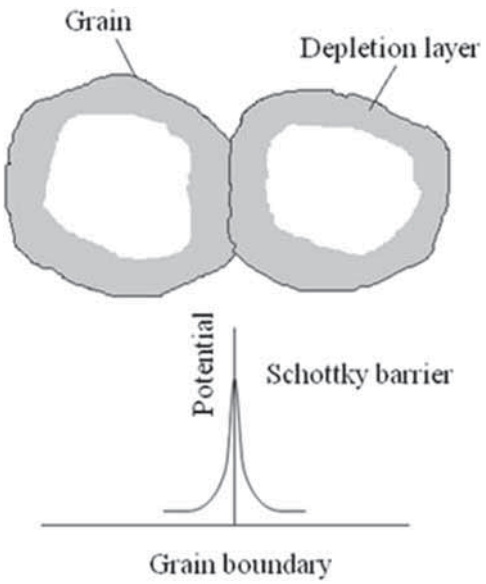

Figure 4. Schematic diagram for grain boundary potential barrier model.

of sensitivity of the sensing elements may be written as given below:

$$\text{Sensitivity} = [(\Delta R)/(\Delta\%\text{RH})] \quad (3)$$

Sensitivity values for the sensing samples ZW-0, ZW-1, ZW-2, ZW-3, ZW-4 and ZW-5 for the annealing temperature 600°C have been calculated and shown in tables 2 and 3. The average sensitivity for the sensing sample WZ-0, ZW-1, ZW-2, ZW-3 and ZW-4 is lower compared to that of sample ZW-5 at the sintering temperature 600°C. As the sintering temperature increases from 300 to 600°C, the sensitivity of the sensing sample ZW-5 increases (table 3). The sample ZW-5 shows results with maximum sensitivity of 12.62, 16.25, 17.12 and 20.95 MΩ/%RH among all samples when annealed at 300, 400, 500 and 600°C, respectively, as shown in figure 5.

4.2 *Humidification and desiccation graphs (hysteresis)*

To determine the hysteresis effect in the sensing elements, first humidity was increased from 15% RH to 95% RH and then cycled down to 15% RH in the humidity chamber, and the values of resistance of the sensing elements were recorded against the variation of %RH. Figure 6 shows hysteresis graph for the sensing element ZW-5 for sintering temperature 600°C. All sensing elements have acceptable hysteresis values. The change in the value of sensitivity in decreasing cycles over increasing cycles for samples ZW-0, ZW-1, ZW-2, ZW-3 and ZW-4 were ±0.10%, ±3.12%, ±2.85%, ±2.71% and ±1.04%, respectively, for the sintering temperature 600°C. Our best sensing element ZW-5 have an acceptable hysteresis values ±1.78%, ±1.63%, ±0.92% and ±0.52% for sintering temperatures 300–600°C. Data sheets of some commercially available humidity sensors indicates hysteresis values in the range from 1.20 to 5.00% [43,44]. The phenomenon of hysteresis may be understood in the manner that due to the adsorption of water on the surface of the sensing element a chemisorbed layer is formed. This chemisorbed layer, once formed is not further affected by exposure to or removal of humidity, it can only be thermally desorbed. Hence, in the decreasing cycle of %RH, the initially adsorbed water is not removed fully, leading to hysteresis.

Thus, the maximum change in the values of sensitivity for the decreasing cycles over increasing cycles for sensing sample WZ-0, WZ-1, WZ-2, WZ-3 and WZ-4 is within the

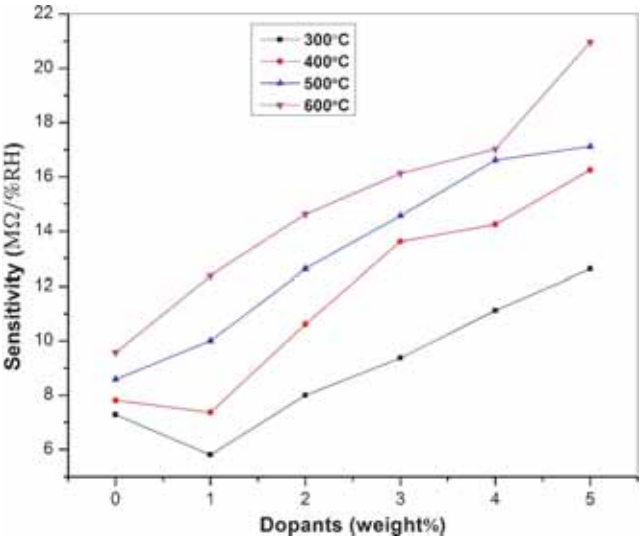

Figure 5. Variation of sensitivity with weight% of ZnO in WO_3.

Table 2. Average sensitivity of sensing elements ZW-0, ZW-1, ZW-2, ZW-3 and ZW-4 for the annealing temperature 600°C in 15–90% RH range.

	Sensitivity MΩ/%RH				
Sensing samples	Increasing cycle	Decreasing cycle	Increasing cycle after 4 months	Increasing cycle after 8 months	% Hysteresis
ZW-0	9.57	9.58	4.88	3.37	0.10
ZW-1	12.38	12.78	9.87	8.87	3.12
ZW-2	14.62	15.05	11.56	10.48	2.85
ZW-3	16.12	16.57	13.1	12.06	2.71
ZW-4	17.02	17.2	14.37	13.37	1.04

Table 3. Average sensitivity of sensing element ZW-5 nanocomposite for different annealing temperatures in 15–95% RH range.

	Sensitivity MΩ/%RH						
Sintering temperature	Increasing cycle	Decreasing cycle	Increasing cycle after 4 months	Increasing cycle after 8 months	% Hysteresis	% Aging 4 Months	% Aging 8 Months
300°C	12.62	12.85	9.68	8.43	1.78	23.29	33.20
400°C	16.25	16.52	13.5	12.5	1.63	16.92	23.07
500°C	17.12	17.28	14.75	13.75	0.92	13.84	19.68
600°C	20.95	21.06	18.62	17.68	0.52	11.12	15.60

range 0.1–3.2% for the sintering temperature 600°C, while for the sensing sample ZW-5 it is within the range 0.5–1.8% for the sintering temperatures 300–600°C.

4.3 *Ageing effect*

Ageing is a significant problem in sensing devices based on metal oxides. To see the aging effect, the sensing elements were kept in laboratory environment and their humidity sensing characteristics were regularly monitored. The sensing properties of the samples were examined again in the humidity chamber after 4 and 8 months and the variation of resistance with %RH recorded. Here, % ageing has been defined as the % deviation in the value of sensitivity over a period of time (for example, 2 months, 8 months, etc.) from the initial measured values. This may be termed repeatability over a period of time as well. The repeatability graph for the sensing element ZW-5 with change in %RH after 4 and 8 months have been shown in figure 7. Corresponding values of sensitivity after 4 and 8 months for sensing elements ZW-0, ZW-1, ZW-2, ZW-3, ZW-4 and ZW-5 are shown in tables 2 and 3. In figure 7, both an initial increasing cycle and another increasing cycle after 4 and 8 months have been shown. We observe that for the sensing sample ZW-5, there is large improvement in reproducibility after 4 and 8 months for the sintering temperature 600°C. Ageing effect present in the ceramic humidity sensor may be due to either prolonged exposure of surface to high humidity, adsorption of contaminants preferentially on the cation sites, loss of surface cations due to vaporization, solubility and diffusion, or sintering to a less reactive structure, migration of cations away from the surface due to thermal diffusion [45,46].

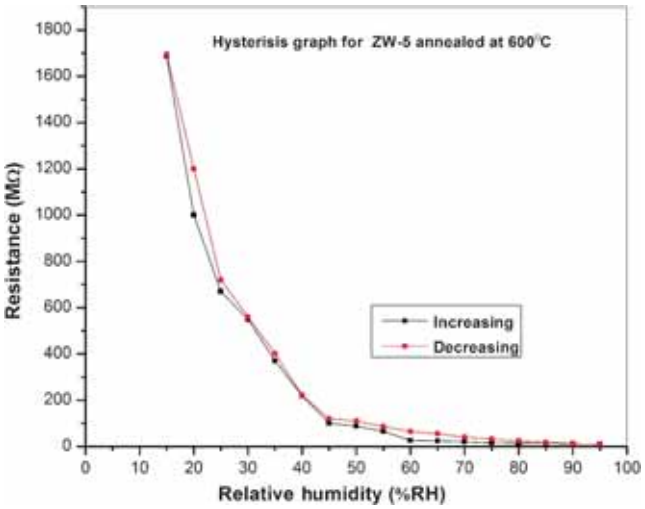

Figure 6. Hysteresis graph for the sample ZW-5 (5% ZnO-doped WO_3) at the sintering 600°C temperature.

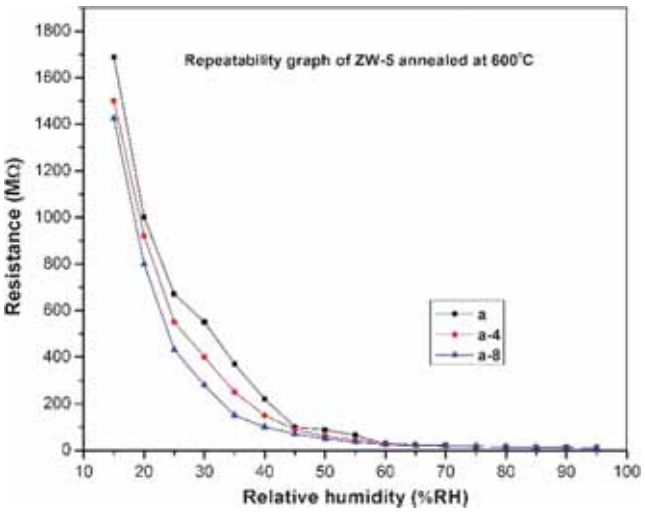

Figure 7. Ageing graph for sensing element ZW-5 (5% ZnO-doped WO_3) for sintering temperature 600°C; **a**: initial humidification cycle of %RH; **a-4**: humidification cycle of %RH after 4 months; **a-8**: humidification cycle of %RH after 8 months.

4.4 *Regression analysis*

Regression analysis of the data was carried out on humidification graphs. Least square fit with respect to polynomials of third degree was established. The coefficients of various power of x (RH) with respect to y (Resistance) are given in table 4. From polynomial of degree 3, value of coefficients of the first power of x are given in table 4; i.e., a_1 is the dominant one, which represents linearity between x and y (RH and resistance). Considering the present state of instrumentation, it is not essential to go for a linear response in sensors; a single valued function should suffice. The nanocomposite qualifies to be a good ceramic humidity sensor with the polynomials of third degree.

4.5 *Response and recovery time*

Time taken to accomplish 90% of the initial total resistance variation is defined as response/recovery time during the humidification and desiccation processes. To find the response and recovery time, the graph shows the variation of resistance with time for sample WZ-5, i.e., the best sample. For sample WZ-5, the response time was 85 s when RH was changed from 15 to 95%, while the recovery time was 550 s when RH was changed from 95 to 15% as shown in figure 8. Adsorption and desorption of the water molecules take place at different energy levels. Adsorption is an exothermic process, where as desorption needs external energy for water

Table 4. Coefficients of various powers of x for polynomial of degree.

Sintering temperature	Polynomial coefficients			
	a_0	a_1	a_2	a_3
300°C	2048.7	−99.811	1.5711	−0.0079
400°C	2709.7	−137.86	2.2214	−0.0114
500°C	2827.6	−133.49	2.044	−0.0101
600°C	3288.6	−147.11	2.1593	−0.0103

molecules to depart from the metal oxide surface. As desorption is an endothermic process, it takes a longer time to desorb the water vapour; therefore, the recovery time is always greater than the response time [47–49].

4.6 *XRD analysis*

XRD has been studied using XPERT PRO-Analytical XRD system (The Netherlands). The wavelength of the source CuKα used is 1.54060 Å. Figure 9 shows the XRD pattern of sensing element WZ-5 annealed at temperature 600°C. The XRD pattern for the sensing element WZ-5 annealed at 600°C shows a lot of WO_3 peaks. High intensity, large number of peaks and sharpness of peaks show high crystallinity of the sensing element WZ-5 annealed at 600°C [50,51]. Some peaks are found broad and the broadness of the peak indicates that crystallites are of small size or nano-size. From Scherer's formula we can see that broader the diffraction peak (i.e., greater the full-width at half-maximum (FWHM) value) smaller the crystal size. XRD pattern for sample ZW-5 shows the monoclinic structure of WO_3 with space group P21/n and the hexagonal structure of ZnO with space group P63mc. Major phase of WO_3 exists for $2\theta = 24.71°$ at the plane (200) and d-spacing corresponding to this peak is 3.60000 Å (figure 9). Scherer's formula gives measurement of crystallite size in sample. Average crystallite size of the samples was calculated using Debye Scherer's formula:

$$D = K\lambda/\beta\cos\theta, \tag{4}$$

where D is the crystallite size, K the fixed number of 0.9, λ the X-ray wavelength, θ the Bragg angle and β FWHM of the peak. The minimum crystallite size calculated from Scherer's formula for the sample ZW-5 is found to be 16 nm. Average crystallite size of sample WZ-5 annealed at 600°C is found to be 48 nm. These crystallites may not be the only factor that affects sensitivity. Crystallites in metal oxides have tendency to agglomerate and form larger grains. The measurement of grain size by SEM for different sintering temperatures was carried out.

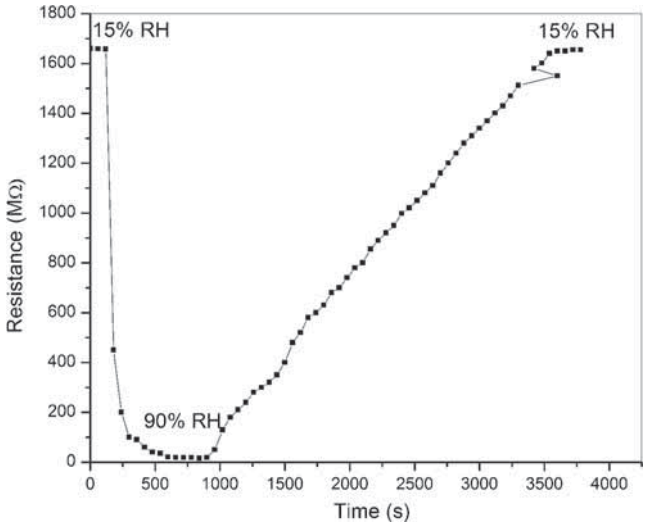

Figure 8. Resistance–time variation graph for sensing element ZW-5.

4.7 *SEM study*

To study the grain micro-structure, SEM micrographs were taken, which would provide a view of the grain development and grain size. SEM micrographs show that porous structure is dependent on the sintering temperature. Sintering at each temperature gives characteristic typical porous structure and small crystallites without inner pores but many intergrain

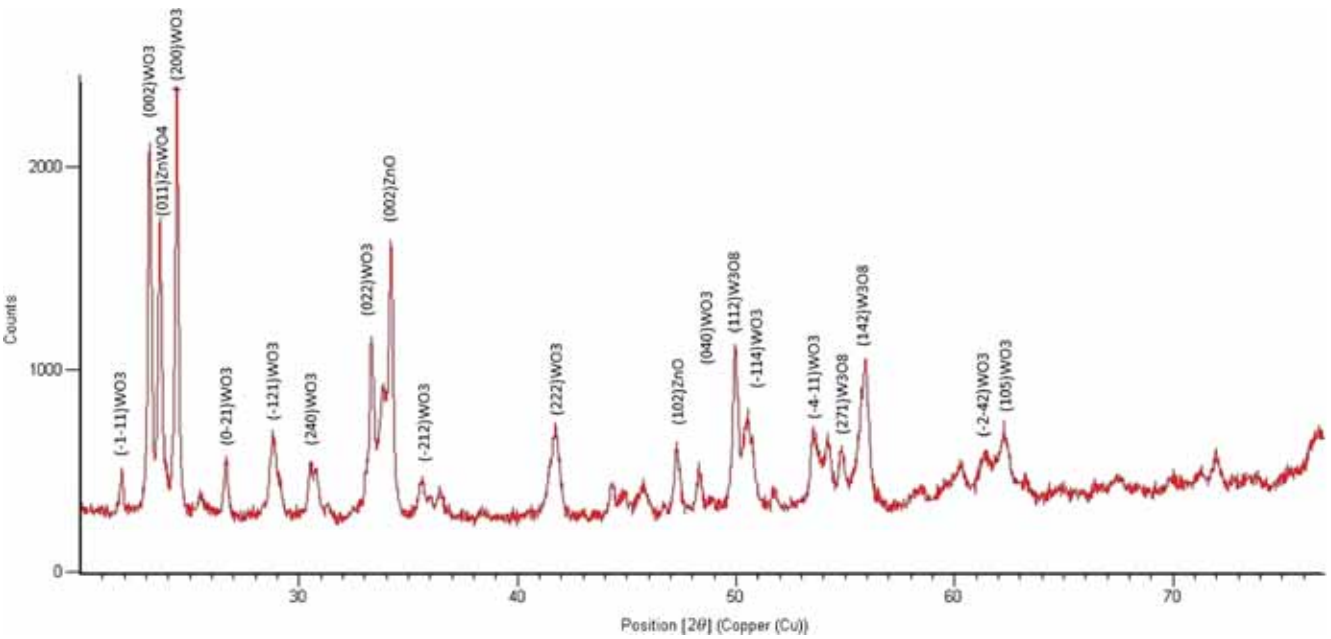

Figure 9. XRD pattern for sensing element of ZW-5 (5% ZnO-doped WO_3) for sintering temperature 600°C.

pores. In addition, it can be observed that intergranular pores are linked through the large pores. The pore structures should be regarded as interconnected voids that form a kind of capillary tube. This structure favours adsorption and condensation of water vapour. Figure 10 shows SEM micrographs of sensing element ZW-5 sintered at temperatures 300, 400, 500 and 600°C. The micrographs were taken at 35.00 KX magnifications. SEM micrographs show that the sensing elements manifest porous structure having granulation and tendency to agglomerate. SEM image, figure 10a, of sensing sample WZ-5 for the sintering temperature 300°C shows highly densely interconnected clusters of small grains (120–180 nm), while figure 10b shows the formation of highly interconnected clusters of small grains (120–240 nm) and densely packed aggregates in sensing sample WZ-5 for the sintering temperature 400°C. When sintering temperature is changed from 400 to 500°C, these dense aggregates grow rapidly and homogeneous grains form (180–240 nm in size) with intergranular pores and capillary pores (figure 10c). At higher temperature 600°C, shown in figure 10d, these grains still grow, such that they form large grains (300–540 nm in size) with larger intragranular pores and a network of capillary pores, which is expected to provide sites for adsorption. As sintering temperature increases, crystallinity of the sensing sample increases and the porosity increases surface-to-volume ratio of the material. Due to the presence of larger grains, more of the surface areas of the sensing elements are exposed leading to more adsorption of water molecules. This increases the sensitivity of the sensing elements.

Arresting particle growth by additives is an established ceramic technique. In general, when the additive ions are not accommodated in the lattice, they tend to segregate at the grain boundaries of host particles. Zn^{2+} having much bigger size (88 pm) than W^{6+} (67 pm) or W^{4+} (68 pm) is not expected to take lattice site. Therefore, it is reasonable to suggest that only a part of the Zn^{2+} takes lattice site for all the compositions, while the remaining part gets segregated at the WO_3 grain boundaries, thus arresting particle growth [52]. With increase in sintering temperature this agglomeration around the host ions increases leading to grain size growth. For sample WZ-5, average grain sizes are 132, 180, 200 and 348 nm for sintering temperatures 300, 400, 500 and 600°C, respectively. As sintering temperature is increased, an evolution in the distribution of the grain size occurs, and that the crystallinity increases with increase in the sintering temperature. The texture and grain size distribution are highly influenced by the increase in sintering temperature. More voids are created during the sintering process. Scanning electron micrographs for sintering temperatures 400 and 500°C manifest a continuity and almost uniform distribution of grains, increasing the formation of voids and interconnected voids or capillaries which are very important conditions for the adsorption of water molecules in the sensing elements. Thus, they will show increasing adsorption capacity for moisture and hence the increasing sensitivity. Sensing element sintered at 600°C has the highest crystallinity as well as the maximum void concentration and porosity. This synergy turns out to be the reason for the affinity towards moisture and hence a higher conductivity. It may be argued that the higher sensitivity may be due to a multiplicative effect of two or more than two parameters of the resultant composite. Samples sintered at lower temperatures may have more

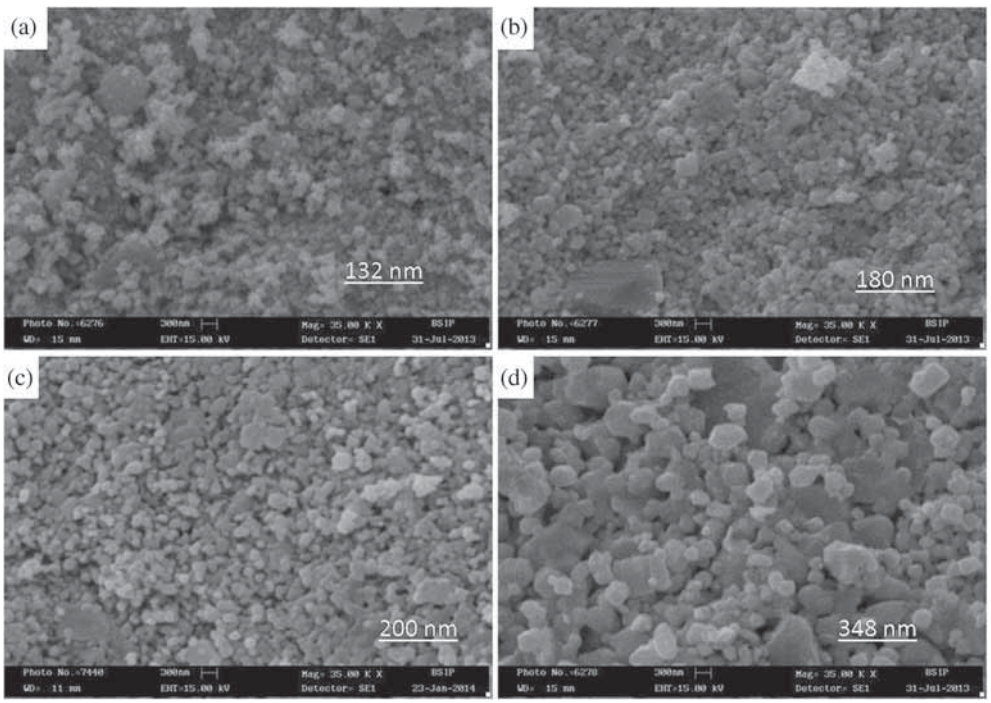

Figure 10. SEM micrograph of sensing element ZW-5 (5% ZnO-doped WO_3) for sintering temperatures (**a**–**d**) 300, 400, 500 and 600°C.

grains per unit area of the surface, yet the range in size of grain is so narrow that the surface of the composite appears smooth and therefore does not provide kinks as adsorption sites [53]. Higher porosity increases surface-to-volume ratio of the materials and therefore, helps in getting good sensitivity. It also helps in reducing response and recovery times because it enhances diffusion rate of water into or out-off the porous structure. An observation of the crystallite size and grain size would suggest that smaller crystallites are getting agglomerated to form larger grains. In this process, more of the surface areas of the sensing elements are exposed leading to more adsorption of water molecules. This increases the sensitivity of the sensing elements.

4.8 *Raman spectroscopy*

Raman scattering is a very sensible tool to examine the structure, phase and components of materials such as tungsten oxides. It is suitable to study the vibration and rotation of molecules. As shown in figure 11, the Raman spectrum of the pure WO_3 and ZnO-doped WO_3 nanostructures sintered at 600°C exhibits five Raman peaks placed at around 134, 275, 327, 715 and 803 cm^{-1}. In Raman spectrum, peaks in the 700–803 cm^{-1} range correspond to the stretching vibrations of W–O bonds while the bands at 275, 327 and lower 200 cm^{-1} correspond to the deformation vibrations of O–W–O bonds, O–W–O bending modes of the bridging oxygen and lattice modes [54]. The peaks at 803 and 715 cm^{-1} are Raman peaks of crystalline WO_3 (m-phase), which correspond to the stretching vibrations of the bridging oxygen [55]. These peaks are attributed to W–O stretching (ν), W–O bending (δ) and O–W–O deformation (γ) modes [56,57]. Figure 11 shows absent of substantial peaks, which means no impurities were present in the samples. The Raman spectra of crystalline WO_3 (WO_3 crystal does not have any double bond) [58,59] as well as all the above information confirms the hypothesis of an open (or porous) structure of the sample with many inner empty spaces and intergrain boundaries. This means the sample is suitable for sensing purpose.

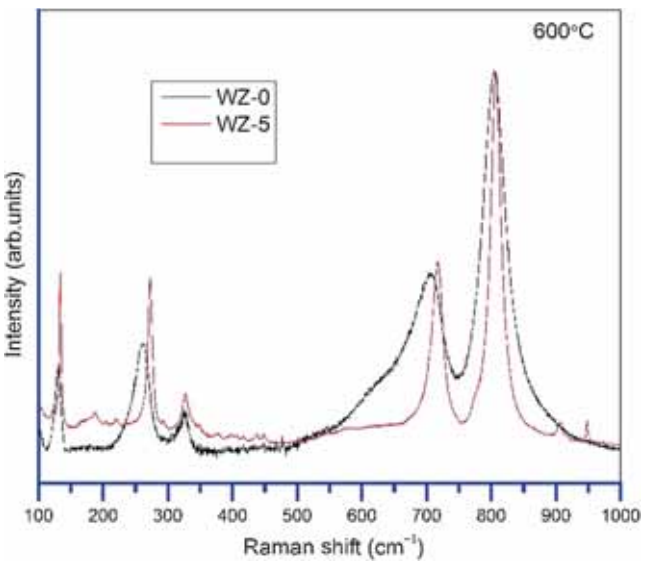

Figure 11. Raman spectra of sensing elements pure WO_3 (ZW-0) and 5% ZnO-doped WO_3 for sintering temperature 600°C.

5. Conclusion

Pure WO_3 and composites with different % doping of ZnO in WO_3 were fabricated and studied for humidity sensing applications. The SEM revealed that WZ-5 composites at annealing temperature 600°C have higher porosity, which increases surface-to-volume ratio of the materials and therefore, helps in getting good sensitivity. It also helps in reducing response and recovery time because it enhances diffusion rate of water into or out-off the porous structure, hence are good candidates for humidity sensors. Among all composites 5 wt% of ZnO–WO_3 composite shows high sensitivity, lower hysteresis and less effect of ageing. Hence our studies suggest that, ZnO–WO_3 composite can be a promising material for high-performance humidity sensing applications.

Acknowledgements

We would like to thank the University Grants Commission, India, for providing the financial support for carrying out the research work through Major Research Project Grant [(file no. 42-788-2013 (SR)]. Thanks are also due for the Geological Survey of India, Lucknow, for providing XRD facility and Birbal Sahni Institute of Paleobotany, Lucknow, for providing SEM facility.

References

[1] Pelino Mario and Cantalini Carlo 1994 *Active and Passive Elec. Comp.* **16** 69

[2] Wang C, Yin L, Zhang L, Xiang D and Gao R 2010 *Sensors* **10** 2088

[3] Akiyama M, Tamaki J, Miura N and Yamazou N 1991 *Chem. Lett.* **9** 1611

[4] Inoue T, Ohtsuka K, Yoshida Y, Matsuura Y and Kajiyama Y 1995 *Sens. Actuators B* **25** 388

[5] Cantalini C, Sun H T, Faccio M, Pelino M, Santucci S, Lozzi L and Passacantando M 1996 *Sens. Actuators B* **31** 81

[6] Sberveglieri G, Depero L and Groppelli S 1995 *Sens. Actuators B* **26** 89

[7] Cantalini C, Pelino M, Sun H T, Faccio M, Santucci S, Lozzi L and Passacantando M 1996 *Sens. Actuators B* **35** 112

[8] Lee D S, Lim J W, Lee S M, Huh J S and Lee D D 2000 *Sens. Actuators B* **64** 31

[9] Chung Y K, Kim M H, Um W S, Lee H S, Song J K, Choi S C, Yi K M, Lee M J and Chung K W 1999 *Sens. Actuators B* **60** 49

[10] Turyan I, Krasovec U O, Orel B, Saraidorov T, Reisfeld R and Mandler D 2000 *Adv. Mater.* **12** 330

[11] Ingham B, Hendy S C, Chong S V and Tallon J L 2005 *Phys. Rev. B* **72** 075109

[12] Kofstad P 1972 *Nonstoichiometry, diffusion, and electrical conductivity in binary metal oxides* (New York: Wiley) p 208

[13] Berak J M and Sienko M J 1970 *J. Solid State Chem.* **2** 109

[14] Yang R, Terabe K, Liu G Q, Tsuruoka T, Hasegawa T, Gimzewski J K and Aono M 2012 *ACS Nano* **6** 9515

[15] Chang T, Jo S H and Lu W 2011 *ACS Nano* **5** 7669

[16] Yang R, Terabe K, Yao Y P, Tsuruoka T, Hasegawa T, Gimzewski J K and Aono M 2013 *Nanotechnology* **24** 384003

[17] Zhao M, Huang J X and Ong C W 2012 *Nanotechnology* **23** 315503

[18] Dai C L, Liu M C, Chen F S, Wu C C and Chang M W 2007 *Sens. Actuators B* **123** 896

[19] Jimenez I, Arbiol J, Dezanneau G, Cornet A and Moronte J R 2003 *Sens. Actuators B Chem.* **93** 475

[20] Kishimoto S, Yamamoto T and Nakagawa Y 2006 *Super Lattices Microstruct.* **39** 306

[21] Yogeeswaran G, Chenthamarakshan C R, Tacconi N R and Rajeshwar K 2006 *Mater. Res. Soc.* **21** 3234

[22] Seghier D and Gislason H P 2008 *J. Mater. Sci. Mater. Electron.* **19** 687

[23] Patil Dewyani, Seo You-Kyong, Hwang Yong Kyu, Chang Jong-San and Patil Pradip 2008 *Sens. Actuators B* **132** 116

[24] Yadav B C, Srivastava Richa and Dwivedi C D 2008 *Philosophical Magazine* **88** 113

[25] Sundaram R and Nagaraja K S 2004 *Mater. Res. Bull.* **39** 581

[26] Guermat Noubeil, Bellel Azzedine, Sahli Salah and Raynaud Patrice 2014 *J. Chem. Sci. Technol.* **3** 13

[27] Md Sin N D, Fuad Kamel M, Alip Rosalena Irma, Mohamad Zulfakri and Rusop M. 2011 *Adv. Mater. Sci. Eng.* **2011** 5

[28] Srivastava Richa and Yadav B C 2012 *Adv. Mat. Lett.* **3** 197

[29] Pandey N K, Tiwari K and Akash R O Y 2012 *Bull. Mater. Sci.* **35** 347

[30] Li Han, Liu Bin, Cai Daoping, Wang Yanrong, Liu Yuan, Mei Lin, Wang Lingling, Wang Dandan, Li Qiuhong and Wang Taihong 2014 *J. Mater. Chem. A* **2** 6854

[31] Pandey N K and Tiwari Karunesh 2010 *Sensors Trans.* **122** 9

[32] Pandey N K, Tiwari Karunesh and Roy Akash 2011 *IEEE Sens. J.* **11** 2911

[33] Pandey N K, Tiwari Karunesh and Roy Akash 2011 *IEEE Sens. J.* **11** 2142

[34] Pandey N K, Tripathi A, Tiwari K, Roy A, Rai A, Awasthi P, Mishra A and Kumar A 2008 *Sensors Trans.* **96** 42

[35] Fleming W J 1981 *Society of automotive engineers transactions* **90** 1656

[36] Seiyama T, Yamazoe N and Arai H 1983 *Sens. Actuators* **4** 85

[37] Yadav B C, Pandey N K, Srivastava Amit K and Sharma Preeti J 2007 *Meas. Sci. Technol.* **260** 18

[38] Frioat J J, Jelli A, Poncele G and André J 1965 *J. Phys. Chem.* **69** 2185

[39] Anderson J H and Parks G A 1968 *J. Phys. Chem.* **72** 3662

[40] Varghese O K and Grimes C A 2003 *J. Nanosci. Nanotechnol.* **3** 277

[41] Qu W and Ray Green M 2000 *Austin, Meas. Sci. Technol.* **11** 1111

[42] Skuratovsky I, Glot A, Di Bartolomeo E, Traversa E and Polini R 2004 *J. Eur. Ceram. Soc.* **24** 2597

[43] Thermoset polymer-based capacitive sensors, application sheet (Online). Available: www.honeywell.com

[44] HIH-3605 Humidity sensor data sheet (Online). Available: www. honeywell.com

[45] Ohbuchi Y, Kawahara T, Okamoto Y and Morimoto J 2001 *J. Appl. Phys.* **40** 213

[46] Saha D, Giri R, Mistry K K and Sengupta K 2004 *Sens. Actuators B Chem.* **107** 323

[47] Saha D, Giri R, Mistry K K and Sengupta K *Sens. Actuators B Chem.* **107** 323

[48] Qu W and Meyer J-U 1997 *Sens. Actuators B* **40** 175

[49] Sundaram R, Raj E S and Nagaraja K S 2004 *Sens. Actuators B* **99** 350

[50] Rout C S, Hegde M and Rao C N R 2008 *Sens. Actuators B* **128** 488

[51] Na Dong-myong, Satyanarayana L., Choi Gwang-Pyo, Shin Yong-Jin and Park Jin Seong 2005 *Sensors* **5** 419

[52] Kim Hye-Kyung, Sathaye Shivaram Dattatraya, Hwang Young Kyu, Jhung Sung Hwa, Hwang Jin-Soo, Kwon Soo Hwan, Park Sang-Eon and Chang Jong-San 2005 *Bull. Korean Chem. Soc.* **1881** 26

[53] Pandey N K, Tiwari K, Roy A, Mishra Aradhana and Govindan Anil 2012 *Int. J. Appl. Ceram. Technol.* **10** 150

[54] Lethy K J, Beena D, Kumar R V, Pillai V P M, Ganesan V, Sathe V and Phase D M 2008 *Appl. Phys. A Mater. Sci. Process* **91** 637

[55] Tagtstrom P and Jansson U 1999 *Thin Solid Films* **352** 107

[56] Daniel F, Desbat B, Lassegues J C, Gerand B and Figlarz M 1987 *J. Solid State Chem.* **67** 235

[57] Shigesato Y, Hayashi Y, Masui A and Haranou T 1991 *Jpn. J. Appl. Phys.* **30** 814

[58] Dixit L, Kapoor S K, Singh I D and Gupta P L 1977 *Indian J. Phys.* **B51** 116

[59] Daniel M F, Desbat B, Lassegues J C and Garie R 1988 *J. Solid State Chem.* **73** 127